THE DIRECTIONAL CHARACTERISTICS OF LUNAR INFRARED RADIATION*

ROMAN U. SEXL**, HANNELORE SEXL**,
HANNS STREMNITZER** and DONALD G. BURKHARD
Department of Physics and Astronomy, University of Georgia, Athens Ga., U.S.A.

(Received 18 March, 1971 †)

Abstract. A theory of the directional characteristics of the lunar infrared radiation measured by Saari and Shorthill has been derived. This theory is in excellent agreement with experiment at all angles of observation and at all phase angles. The radiation law used to describe the angular dependence of the infrared radiation emitted by a flat element of the lunar surface is $0.85\cos\theta + 0.22\cos^2\theta$, where θ is the angle between the surface normal and the direction of observation. This radiation law is subsequently modified by taking into account lunar surface roughness. We assume a surface covered in part with spherical craters of various depth to diameter ratios as a model for the lunar soil. Re-radiation within the craters has been accounted for. Extensive use is made of group theoretical and invariant tensor methods which enable us to show that most of the details of the radiation pattern do not depend on the detailed nature of the surface features assumed, but only on the average surface slope. A best fit to the Saari-Shorthill data has been obtained by assuming 50% of the lunar surface to be covered with craters with a depth to diameter ratio of 1:3, while the remainder of the surface is essentially flat. The mean deviation between theory and experiment is 4K.

1. Introduction

The directional characteristics of the lunar infrared radiation have been measured with great precision by Saari and Shorthill (1967). These measurements show that the thermal radiation emitted by the Moon is strongly anisotropic. The most characteristic feature of the infrared radiation is that it is radiated predominantly in the direction of the incident solar light under most conditions.

Smith (1967) has attempted to explain the strong anisotropy of the radiation with the help of a statistical model of lunar roughness. Excellent agreement has been obtained when comparison was made with the variation of the subsolar radiance with phase. No agreement was obtained, however, when comparison was made with the full moon data.

A drawback of Smith's method is, furthermore, that no general expression has been obtained for the lunar infrared radiation and that separate calculations are necessary for each phase.

Buhl *et al.* (1968) have used a different approach. They considered the effects of craters in altering the emission characteristics of the lunar surface. However, only

* This work has been supported by the National Aeronautics and Space Administration under Contracts No. NAS8-20385 and NAS8-25585, Marshall Space Flight Center, Alabama.
** Permanent Address: Institut für Theoretische Physik, Universität Wien, 1090 Wien, Boltzmanngasse 5, Austria.
† Receipt delayed due to postal strike in Great Britain.

The Moon 3 (1971) 189–213.

the radiation emitted by the subsolar point and at full Moon have been studied in this paper.

Winter and Krupp (1970) have made a very detailed and thorough analysis of the Saari-Shorthill data and have obtained the emission characteristics of a cratered surface using various crater distributions and shapes. Only points along the lunar equator have been considered in Winter and Krupp (1970) and good agreement with the experimental data has been obtained. The theoretical papers quoted above possess in common the feature that a Lambertian cosine-law has been used to describe the directional characteristics of a uniformly heated flat surface consisting of lunar material. There is no reason for this assumption to hold. Electromagnetic theory predicts that a uniformly heated dielectric radiates predominantly in the direction of the surface normal, although the exact amount of this enhancement is difficult to calculate.

Here we shall generalize the model by modifying the basic ansatz for the radiation law. A parameter r has been introduced to describe deviations from the Lambert law, which might exist even for a flat lunar surface element. This radiation law is subsequently modified by taking into account the roughness of the lunar surface.

The approach presented here differs from previous work, furthermore, by the extensive use of group theoretical and invariant tensor methods. These methods enable us to calculate the radiation emitted by a cratered surface in closed analytic form. The theoretical methods used here enable us, furthermore, to determine which features of the radiation pattern are model dependent: i.e. depend on the details of the crater distribution, shape etc. It turns out that the thermal behaviour of the rim of the lunar disk is the only feature of the radiation patterns which depends strongly on these details while the bulk of the data is influenced only by the rms slope of the surface and insensitive to the detailed form of the surface roughness.

Another advantage of our method is that we are able to calculate lunar temperatures also off-equator and are thus in a position to fit all Saari Shorthill data with a single theoretical formula.

The outline of our paper is the following: Section 2 summarizes the relevant aspects of previous work and contains a detailed analysis of the energy balance. Section 3 deals with the radiation emitted by unshadowed craters. In this section the group-theoretical method is developed and explained in detail. In Section 4 our model is specialized to spherical craters, and in Section 5 we calculate the re-radiation effects in such craters. The very complicated shadowing effects are considered in detail in Section 6 and closed form mathematical expressions are derived for the radiation emitted by shadowed craters. In Section 7 we compare our theory with experiment and it turns out that excellent agreement with the experimental data can be reached for a surface covered in part (50%) with craters with depth to diameter ratio $=1:3$.

2. The Energy Balance

In this section we shall study the question of the energy balance at the lunar

surface in detail, starting with a review of the work of Ashby (1966) on the influence of the thermal conductivity and the lunar albedo on the infrared radiation. In Table I we have listed the energy received per unit surface in the form of solar light, the energy reflected optically and the energy lost by thermal conduction as functions of the thermal latitude β (see Figure 1 for the definition of angles). The table shows that optical reflection accounts for 5% of the energy, 1% is transported

TABLE I

Energy balance

All energies in cal/cm² min				
β	$S\sin\beta$	R	C	I
90	1.99	0.096	0.010	1.88
85	1.98	0.096	0.010	1.87
80	1.96	0.095	0.011	1.85
75	1.92	0.093	0.011	1.82
70	1.87	0.091	0.011	1.77
65	1.80	0.088	0.012	1.70
60	1.72	0.085	0.012	1.62
55	1.63	0.081	0.012	1.54
50	1.52	0.076	0.012	1.43
45	1.40	0.071	0.012	1.32
40	1.28	0.065	0.011	1.20
35	1.14	0.059	0.010	1.07
30	1.00	0.0516	0.009	0.937
25	0.840	0.0437	0.007	0.786
20	0.681	0.0352	0.006	0.630
15	0.515	0.0260	0.004	0.485
10	0.346	0.0162	0.001	0.329
5	0.173	0.0063	0.001	0.168

R – Reflected energy,
C – Conducted energy
I – Infrared energy

by thermal conduction and 94% are available for thermal radiation. In our work we shall attempt to predict temperatures with an accuracy of about ± 3 K, corresponding to an accuracy of about 3% in the energy balance. Therefore, we can neglect the influence of thermal conduction on the energy balance, which is rather fortuitous; since the conductivity loss depends not only on the thermal latitude β, but also on the thermal longitude ψ. The values quoted in the table are averages over the longitude.

Subtracting the conduction and reflection losses from the incident energy $S\sin\beta$ ($S = 1.99$ cal/cm² min is the solar constant) we see that the energy available for thermal radiation is given to a high degree of accuracy by $S_c \sin\beta$, where $S_c = 1.88$ cal/cm² min is the solar constant corrected for conduction and reflection. This result is rather fortuitous, since it enables us to take into account the two other energy transfer processes in a rather simple manner. It has to be emphasized, however, that

the expression $S \sin\beta$ for the incident solar energy arises from purely geometrical considerations, while the approximate expression for the net energy $S_c \sin\beta$ available for thermal radiation is the result of rather involved calculations.

In order to proceed further with the check of the energy balance we have to introduce several unit vectors and the angles between them so that the directional characteristics of the infrared radiation can be expressed in convenient form. The necessary

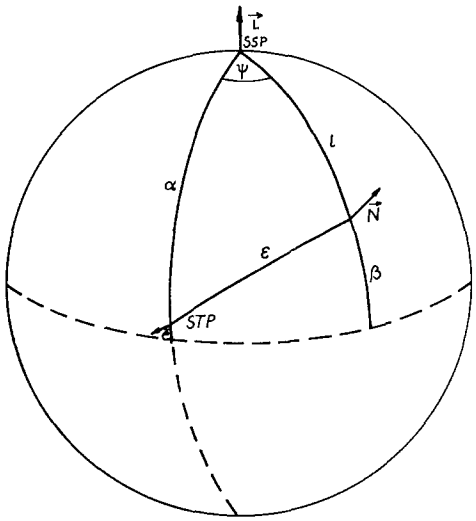

Fig. 1. Definition of thermal coordinates.

details are contained in Figure 1. **N** is a unit vector orthogonal to the lunar surface element considered (after averaging over local irregularities), **i** points in the direction of the Sun and **e** is a unit vector in the direction of the emitted radiation. The following relations between the scalar products of these vectors and the angles defined in Figure 1 hold:

$$\cos\iota = (\mathbf{i}\cdot\mathbf{N}) = \sin\beta, \tag{2.1}$$

$$\cos\varepsilon = (\mathbf{e}\cdot\mathbf{N}), \tag{2.2}$$

$$\cos\alpha = (\mathbf{i}\cdot\mathbf{e}), \tag{2.3}$$

ι, ε and α are the angle of incidence, angle of observation and phase angle resp. ε can be expressed in terms of ι, α and the thermal longitude ψ as

$$\cos\varepsilon = \cos\alpha\cos\iota + \sin\alpha\sin\iota\cos\psi\,. \tag{2.4}$$

With the aid of these definitions the energy balance reads

$$E_t = \int \mathrm{d}\Omega\, E(\varepsilon, \iota, \alpha) = S_c \cos\iota\,, \tag{2.5}$$

where E_t is the total infrared energy radiated by a unit surface element and $E(\varepsilon, \iota, \alpha)$ is the radiation emitted in the direction **e** per unit solid angle.

The energy flux E observed experimentally (with a telescope of fixed aperture) is connected with $E(\varepsilon, \iota, \alpha)$ by

$$E_{\text{obs}} = E(\varepsilon, \iota, \alpha)/\cos\varepsilon . \tag{2.6}$$

The factor $1/\cos\varepsilon$ takes into account the variation of the lunar area observed with the angle ε of observation.

The temperature T of a given surface element can be related to the infrared radiation emitted with the help of the Stefan-Boltzmann law

$$E_t = \sigma T^4 \tag{2.7}$$

(σ is the Stefan-Boltzmann constant).

For a Lambertian radiator the energy flux radiated per unit solid angle is proportional to $\cos\varepsilon$ and the observed energy is thus a constant independent of the angle of observation, according to (2.6). In this case a simple relation holds between E_t and the observed energy E_{obs}

$$E_t = \int \mathrm{d}\Omega\, E(\varepsilon, \iota, \alpha) = 2\pi \int \mathrm{d}(\cos\varepsilon)\, E_{\text{obs}} \cos\varepsilon = \pi E_{\text{obs}} \tag{2.8}$$

and the temperature can, therefore, be defined in terms of the energy flux observed as

$$T^4 = \frac{\pi}{\sigma} E_{\text{obs}} . \tag{2.9}$$

For a non-Lambertian radiator, such as the lunar surface, (2.9) can be used to define effective temperatures by

$$T^4(\varepsilon, \iota, \alpha) = \frac{\pi}{\sigma} E_{\text{obs}} = \frac{\pi E(\varepsilon, \iota, \alpha)}{\sigma \cos\varepsilon} . \tag{2.10}$$

This effective temperature, which depends both on the angle of incidence and the phase angle, has been measured by Saari and Shorthill (1967) and will be calculated here from a theoretical model.

Assuming the Moon to be a Lambertian radiator one easily calculates the temperature of the subsolar point from (2.5 and 7) to be

$$T = (S_c/\sigma)^{1/4} = 390\,K . \tag{2.11}$$

The apparent temperature at the center of the lunar disk at full Moon as measured by Saari and Shorthill is, however,

$$T = 397\,K . \tag{2.12}$$

This enhancement of the subsolar radiation at $\varepsilon = 0$ has to be compensated by a corresponding lowering of the apparent temperature at large ε in order to maintain

the energy balance. This effect is shown in Figure 2. The value (2.12) is in fact derived from such energy balance considerations rather than from direct experimental evidence since the absolute calibration of the bolometers used to measure $T(\iota, \varepsilon, \alpha)$ is an extremely complicated task.

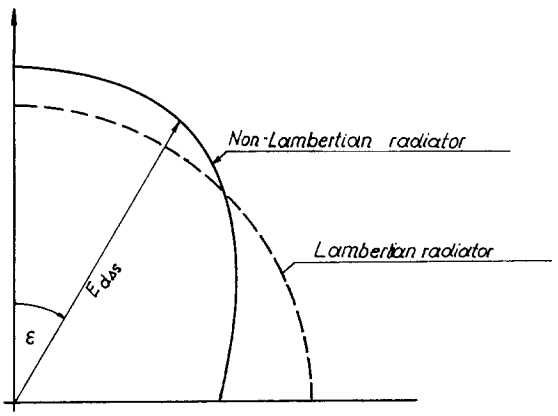

Fig. 2. Polar plot of lunar heat from the subsolar point for a Lambertian and non-Lambertian radiator.

The older value $T=407\,\mathrm{K}$ for the centrilunar temperature at full Moon is incorrect, since Pettit and Nicholson (1930) have omitted the second factor $\cos\varepsilon$ contained in (2.8) in their work, leading to an incorrect energy balance and to an overprediction of all lunar temperatures.

3. Thermal Radiation from a Rough Surface

In this section we shall start our calculation of the directional characteristics of the infrared radiation emitted by a rough surface illuminated by a light source at an angle of incidence ι. We shall show that the radiation pattern can be calculated quite generally for a surface with arbitrary slope distribution for angles of observation and incidence such that no part of the surface is shadowed (i.e. invisible from the light source) or invisible from the direction of observation. In this case no detailed assumptions about the surface features are necessary, except that no preferred directions exist on the surface when one averages over sufficiently large areas.

In order to calculate the radiation emitted by a rough surface we have to start with an assumption about the radiation emitted by an infinitesimal flat surface element. Usually one assumes this radiation to be Lambertian. There is, however, no reason for this assumption to hold for the lunar surface. Electromagnetic theory predicts that the radiation emitted by a dielectric will be peaked more towards the surface normal than the Lambert law predicts.

We shall therefore assume that a flat element of the lunar surface radiates with an

angular distribution proportional to

$$\varrho(\mathbf{e}, \mathbf{n}) = \frac{1}{\pi}\{(1-r)(\mathbf{e}\cdot\mathbf{n}) + \frac{3}{2} r(\mathbf{e}\cdot\mathbf{n})^2\}, \tag{3.1}$$

where $\mathbf{n}$ is the local surface normal (i.e. $\mathbf{n}$ is orthogonal to the infinitesimal surface element rather than to the mean lunar surface), $(\mathbf{e}\cdot\mathbf{n}) = \cos\theta$ is the scalar product of $\mathbf{n}$ with the unit vector $\mathbf{e}$ in the direction of observation*. The constant r describes the deviations of the radiation law used here from a purely Lambertian cos-law, which would be obtained for $r=0$. The representation (3.1) for the radiation law can be considered as the first terms of a systematic expansion in terms of $\cos\theta$ and higher terms can be added if necessary. The coefficients in (3.1) have been chosen in such a way that the angular distribution of the radiation is normalized to one: i.e.,

$$\int \mathrm{d}\Omega_e \, \varrho(\mathbf{e}, \mathbf{n}) = 1. \tag{3.2}$$

This normalization is independent of the value of r. The non-Lambertian parameter r could be determined experimentally by measuring the distribution of the radiation emitted by the lunar surface material gathered during the Apollo 11 and 12 flights; the experiment has not yet been performed, however.

The energy available for thermal radiation by an infinitesimal element $\mathrm{d}f$ of the lunar surface is given by $S_c(\mathbf{i}\cdot\mathbf{n})\,\mathrm{d}f$, as discussed in the previous section. This energy is then radiated according to (3.1) with an angular distribution

$$\mathrm{d}f \; E(\mathbf{e}, \mathbf{i}, \mathbf{n}) = S_c \, \mathrm{d}f \, (\mathbf{i}\cdot\mathbf{n}) \, \varrho(\mathbf{e}, \mathbf{n}); \tag{3.3}$$

$E(\mathbf{e}, \mathbf{i}, \mathbf{n})$ is, therefore, the infrared energy emitted by a flat unit surface per unit solid angle and unit time. Energy is conserved because of (3.2), which leads to

$$\int \mathrm{d}\Omega_e \, E(\mathbf{e}, \mathbf{i}, \mathbf{n}) = S_c(\mathbf{i}\cdot\mathbf{n}). \tag{3.4}$$

We turn now to the problem of calculating the radiation emitted by a rough surface. We have to integrate the radiation emitted by each surface element over a finite surface area with varying surface normal $n(f)$, where f stands for the surface element considered (see Figure 3). The total radiation emitted by the surface becomes

$$F \, E(\mathbf{e}, \mathbf{i}, \mathbf{N}) = \frac{S_c}{\pi} \int \mathrm{d}f \, (\mathbf{i}\cdot\mathbf{n}) \{(1-r)(\mathbf{e}\cdot\mathbf{n}) + \frac{3}{2} r(\mathbf{e}\cdot\mathbf{n})^2\}, \tag{3.5}$$

where $\mathbf{N}$ is the average surface normal and F is the total apparent surface, both shown in Figure 4. This integral can be evaluated rigorously for arbitrary slope distributions. Figure 3 shows, however, that (3.5) will not be the exact expression for the radiation because of two reasons:

* $\cos\theta = (\mathbf{e}\cdot\mathbf{n})$ differs from $\cos\varepsilon = (\mathbf{e}\cdot\mathbf{N})$, $\mathbf{N}$ being the mean surface normal.

(1) Parts of the surface will be invisible and/or shadowed. These parts of the surface should be omitted in the integral (3.5).

(2) Re-radiation effects exist. The radiation emitted by one surface element can be absorbed and subsequently re-emitted in a different direction by another surface element.

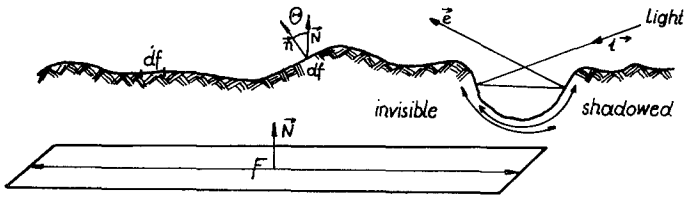

Fig. 3. Local and global surface normal. Re-radiation is shown at right.

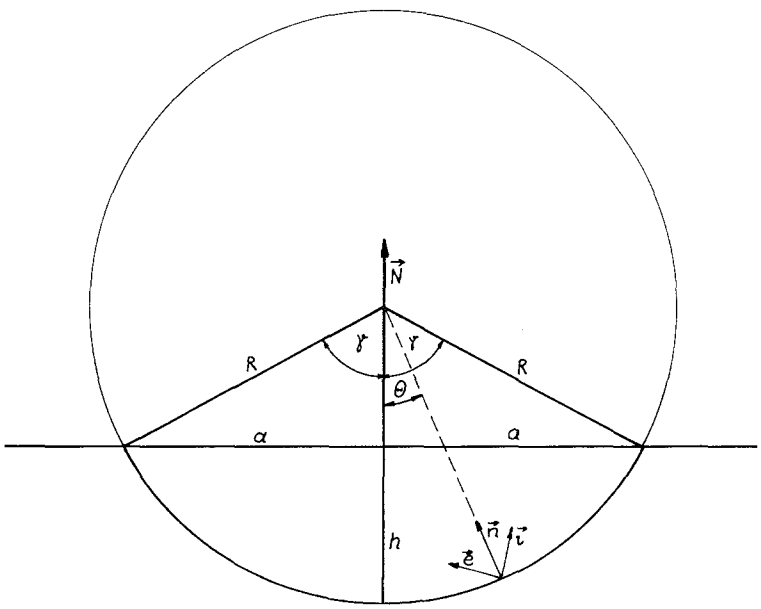

Fig. 4. Geometry of spherical craters.

Both effects will be neglected in this section and studied in detail in Sections 4–6 of this paper. Here we shall show how the integral (3.5) can be evaluated with the help of group theoretical methods if the integration is extended over a part of the surface which is sufficiently large so that no preferred directions exist on it. This is true for a surface covered with circular craters or hills (if one integrates over an area containing many craters), but also for much more general surface types covered e.g. with linear ridges, if these ridges are not aligned in one dominant direction. This assumption is certainly fulfilled for the lunar surface, if we integrate in (3.5) over the surface areas (several square miles) which contribute to the Saari-Shorthill (1967) data points. To evaluate (3.5) we introduce tensor notation and denote the com-

ponents of the unit vector **n** by n_i, $i = 1, 2, 3$ etc. Then (3.5) can be rewritten as

$$E(\mathbf{e}, \mathbf{i}, \mathbf{N}) = \frac{S_c}{F\pi} \{(1 - r)\, i_k e_m \int \mathrm{d}f\; n_k n_m + \frac{3r}{2}\, i_k e_m e_r \int \mathrm{d}f\; n_k n_m n_r\}\,. \tag{3.6}$$

In (3.6) the Einstein sum convention has been used, i.e. a sum over each index that appears twice in (3.6) is implied. Therefore a typical scalar product is written as $(\mathbf{n}\cdot\mathbf{e}) = n_k e_k \equiv \sum_{k=1}^{3} n_k e_k$. The two integrals appearing in (3.6) can depend only on the average surface normal **N**, since no other preferred directions exist on the lunar surface. Therefore we can express the first integral appearing in (3.6) in the form

$$\int \mathrm{d}f\; n_k n_m = a_1 N_k N_m + a_2 \delta_{km}\,, \tag{3.7}$$

where a_1 and a_2 are two constants to be determined. δ_{km} is the Kronecker symbol (unit matrix). It is immediately obvious that the two terms contained in (3.7) are the only symmetric tensors of rank two that can be formed from N_k and the unit matrix. A formal proof can be given using group theory (Hammermesh, 1962).

The second integral contained in (3.6) can be expressed in the form

$$\int \mathrm{d}f\; n_k n_m n_r = b_1 N_k N_m N_r + b_2 (\delta_{km} N_r + \delta_{kr} N_m + \delta_{mr} N_k)\,, \tag{3.8}$$

where the two constants b_1 and b_2 have to be determined.

Inserting (3.7) and (3.8) into (3.6) we obtain

$$\begin{aligned} E(\mathbf{e}, \mathbf{i}, \mathbf{N}) = \frac{S_c}{F\pi} \{&(1 - r)\, a_1 (\mathbf{i}\cdot\mathbf{N})(\mathbf{e}\cdot\mathbf{N}) + a_2 (1 - r)(\mathbf{i}\cdot\mathbf{e}) \\ &+ \frac{3r}{2}\, b_1 (\mathbf{i}\cdot\mathbf{N})(\mathbf{e}\cdot\mathbf{N})^2 + \frac{3r}{2}\, b_2 [2(\mathbf{i}\cdot\mathbf{e})(\mathbf{e}\cdot\mathbf{N}) + (\mathbf{i}\cdot\mathbf{N})]\}\,. \end{aligned} \tag{3.9}$$

We are thus able to express the directional characteristics of the radiation emitted by a rough surface in terms of 4 constants, which have to be evaluated in terms of the surface roughness. For this purpose we first put $k = m$ in (3.7) and sum over this index, secondly we multiply (3.7) by $N_k N_m$. The result is

$$\begin{aligned} \int \mathrm{d}f\; (\mathbf{n}\cdot\mathbf{N})^2 &= a_1 + a_2\,, \\ \int \mathrm{d}f\; &= a_1 + 3a_2\,. \end{aligned} \tag{3.10}$$

Similarly we can contract (3.8) with $N_k N_m N_r$ and $\delta_{mk} N_r$ and obtain

$$\begin{aligned} \int \mathrm{d}f\; (\mathbf{n}\cdot\mathbf{N})^3 &= b_1 + 3b_2\,, \\ \int \mathrm{d}f\; (\mathbf{n}\cdot\mathbf{N}) &= b_1 + 5b_2\,. \end{aligned} \tag{3.11}$$

In these equations $(\mathbf{n}\cdot\mathbf{N})=\cos\theta$ is the local surface slope. The constants a_1, a_2, b_1, b_2 can thus be expressed in terms of the surface moments

$$c_m = \frac{1}{f}\int \mathrm{d}f\,(\mathbf{n}\cdot\mathbf{N})^m = \frac{1}{f}\int \mathrm{d}f\,(\cos\theta)^m = \overline{\cos^m\theta}, \tag{3.12}$$

where the bar denotes an average over the surface considered. The c_m are thus the average values of the m-th power of the surface slope. c_1 has a simple geometrical interpretation since

$$c_1 = \frac{1}{f}\int \mathrm{d}f\,\cos\theta = F/f\,, \tag{3.13}$$

where F is the apparent surface while f is the total surface area (see Figure 3). If we express all constants in terms of F and c_m we obtain

$$\begin{aligned} a_1 &= F(3c_2 - c_0)/2c_1\,, \quad & a_2 &= F(1-c_2)/2c_1\,, \\ b_1 &= F(5c_3 - 3c_1)/2c_1\,, \quad & b_2 &= F(c_1 - c_3)/2c_1\,. \end{aligned} \tag{3.14}$$

Inserting these results into (3.9) we obtain a general expression for the radiation emitted by a rough surface. The main advantage of the group theoretical method used here over standard calculations is thus that it shows that the main contributions to the radiation law (we will have to augment (3.9) by model dependent reradiation and shadowing contributions) are model independent and can be expressed in terms of the surface moments. These surface moments c_n will be calculated for a special model surface in the next section.

4. Geometry of Spherical Craters

The model of the lunar surface used here agrees with the one used by Winter and Krupp (1970) and Buhl *et al.* (1968). We consider the lunar surface as covered in part by spherical craters of various depth to diameter ratios, as shown in Figure 4. To describe the crater geometry it is useful to introduce the parameter

$$s = h/2R\,, \tag{4.1}$$

i.e. the ratio of the depth of the crater to the diameter of the sphere of which it is part. The quantity s is related to the opening angle γ of the crater (see Figure 4) by $s=\sin^2(\gamma/2)$. The radius a of the spherical crater rim becomes in terms of s

$$a = R\sin\gamma = 2R\sqrt{s(1-s)}\,. \tag{4.2}$$

The total crater area is given by

$$f = R^2\int_0^{2\pi}\mathrm{d}\phi\int_0^{\gamma}\sin\theta\,\mathrm{d}\theta = 4\pi R^2 s\,, \tag{4.3}$$

while the apparent surface area follows from (4.2) to be

$$F = a^2\pi = 4\pi R^2 s(1-s)\,. \tag{4.4}$$

The calculation of the surface moments c_m of the crater is easiest in polar coordinates:

$$c_m = \frac{1}{f}\int \mathrm{d}f\,(\mathbf{n}\cdot\mathbf{N})^m = \frac{2\pi R^2}{4\pi R^2 s}\int_{\cos\gamma}^{1} \mathrm{d}(\cos\theta)\cos^m\theta \tag{4.5}$$
$$= [1-(1-2s)^{m+1}]/2s(m+1).$$

From $c_2 = 1-2s+0(s^2)$ we obtain $s \approx \frac{1}{2}\overline{\sin^2\theta}$, and thus a simple interpretation of s in terms of the rms surface slope. Inserting (4.5) into (3.14) and (3.9) we obtain for the radiation emitted by a single crater

$$E(\mathbf{e},\mathbf{i},\mathbf{N}) = \frac{S_c}{\pi}\{\cos\alpha(1-r)\,s\,\frac{1-2s/3}{1-s} + (1-r)\cos\varepsilon\cos\iota(1-2s)$$
$$+\frac{3rs}{2}(1-s)\cos\iota + 3rs(1-s)\cos\alpha\cos\varepsilon \tag{4.6}$$
$$+\frac{3r}{2}(1-5s+5s^2)\cos\iota\cos^2\varepsilon\}.$$

This is the main result of our group-theoretical treatment of the lunar infrared radiation. In the following sections this result will be modified by taking into account shadowing effects and re-radiation.

5. Re-radiation Corrections

In this section we evaluate the contribution of the radiation which is emitted by one part of the crater surface, absorbed by an other part and subsequently reemitted. We shall assume here that no part of the crater is shadowed.

We shall calculate the re-radiation in terms of an infinite series, which will turn out to be a geometrical series and can, therefore, be summed exactly. This series is, of course, the Friedmann series of the integral equation for radiative heat transfer.

The geometrical situation is shown in Figure 5. $\mathbf{e}$, $\mathbf{i}$, $\mathbf{e}_{01}$, $\mathbf{n}_1$, $\mathbf{n}_0$ are unit vectors in

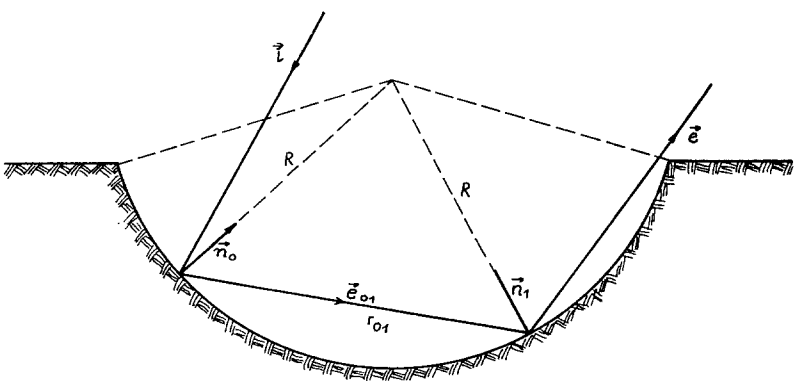

Fig. 5. Re-radiation corrections.

the directions indicated. The radiation emitted in the direction **e** after one absorption is given by

$$d^{(1)} E(\mathbf{e}, \mathbf{i}, \mathbf{N}) = S_c \iint \mathrm{d}f_0 (\mathbf{i} \cdot \mathbf{n}_0) \varrho(\mathbf{e}_{01}, \mathbf{n}_0) \frac{(\mathbf{e}_{01} \cdot \mathbf{n}_1)}{r_{01}^2} \varrho(\mathbf{e}, \mathbf{n}_1) \mathrm{d}f_1/F . \quad (5.1)$$

This expression can be simplified, using

$$(\mathbf{e}_{01} \cdot \mathbf{n}_0) = (\mathbf{e}_{01} \cdot \mathbf{n}_1) = r_{01}/2R . \quad (5.2)$$

Then the integral (5.1) can be evaluated approximately to be

$$\mathrm{d}^{(1)} E(\mathbf{e}, \mathbf{i}, \mathbf{N}) = \frac{S_c}{\pi} K(1-s) \cos\iota \{(1-r)\cos\varepsilon + \frac{3rs(1-2s/3)}{2(1-s)} + \frac{3r}{2}\cos^2\varepsilon(1-2s)\} . \quad (5.3)$$

In (5.3) terms of order $rs^{5/2}$ and smaller terms have been neglected; they contribute very little ($<0.2\%$) to the radiation since r and s are assumed to be small. The constant K is given by

$$K = s[(1-r) + \frac{3r}{2}\sqrt{s(1-s)}(1-s)^2] . \quad (5.4)$$

The calculation of terms of higher order is straightforward. The contribution of the n-th order becomes

$$\mathrm{d}^{(n)} E = S_c \int \mathrm{d}f_0 \ldots \int \mathrm{d}f_n (\mathbf{i} \cdot \mathbf{n}_0) \varrho(\mathbf{e}_{01}, \mathbf{n}_0) \frac{(\mathbf{e}_{01} \cdot \mathbf{n}_1)}{r_{01}^2} \varrho(\mathbf{e}_{12}, \mathbf{n}_1) \times \frac{(\mathbf{e}_{12} \cdot \mathbf{n}_2)}{r_{12}^2} \ldots \varrho(\mathbf{e}, \mathbf{n}_n)/F . \quad (5.5)$$

This can be evaluated as before and differs from the first order contribution only by extra powers of K. Therefore a geometrical series results and the total re-radiation contribution becomes

$$E^r(\mathbf{e}, \mathbf{i}, \mathbf{N}) = \mathrm{d}^{(1)} E(\mathbf{e}, \mathbf{i}, \mathbf{N})/(1-K) . \quad (5.6)$$

This term has to be added to (4.6).

6. Shadowing

We turn now to the case that part of the crater is either shadowed or invisible. Since both situations show many similarities we shall treat them here together and use the name shadowing for both effects. Whenever necessary we shall distinguish between actual and apparent shadowing (invisibility).

Actual shadowing occurs whenever the angle of incidence ι exceeds a critical value such that

$$\cos\iota < \sin\gamma = \sqrt{4s(1-s)} . \quad (6.1)$$

In this case part of the crater will be shadowed.

Apparent shadowing occurs when the angle of observation exceeds the same critical value i.e.,

$$\cos\varepsilon < \sin\gamma\,. \tag{6.2}$$

In general both actual and apparent shadowing will occur and 4 different situations can arise as shown in Figure 7:

(a) Only actual or apparent shadowing is present.
(b) Apparent and actual shadows do not overlap.
(c) Apparent and actual shadows overlap completely.
(d) The shadows overlap in part.

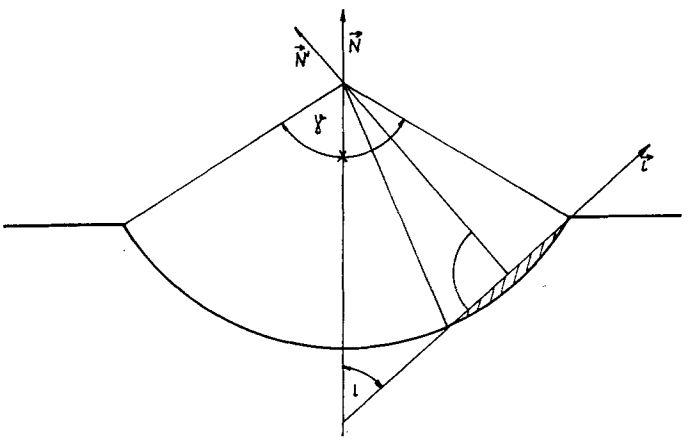

Fig. 6. Geometry of shadowing.

Case (d) is the most complicated one and can be dealt with only approximately. This will be done later. In case (c) only the larger one of the two shadows has to be taken into account and therefore the situation will be analogous to (a). Case (b) can be obtained from (a) by subtracting the 2 independent contributions of the two shadows from the total radiation.

We shall therefore treat (a) first. For simplicity we shall concentrate on actual shadowing; apparent shadowing can be derived therefrom by replacing ι by ε in all equations. Figure 6 shows the geometrical configuration. It is well known that the area shadowed inside a spherical crater is bounded by a segment of a circle, the radius of which equals the radius a of the crater rim. This can also be read off Figure 6 by observing the symmetry of the figure with respect to the direction $\mathbf{N}'$.

It will turn out to be convenient to introduce a new coordinate system with the Z-axis pointing in the direction $\mathbf{N}'$, while the X-axis lies in the direction of the incident light (see Figure 6). The tripel of mutually orthogonal unit vectors $(\hat{\mathbf{X}}, \hat{\mathbf{Y}}, \hat{\mathbf{Z}})$ pointing in the directions of the X, Y, Z-axis of the new coordinate system is given by

$$(\hat{X}, \hat{Y}, \hat{Z}) = (\mathbf{i}, \mathbf{N} \times \mathbf{i}/\sin\iota, (\mathbf{N} - \mathbf{i}\cos\iota)/\sin\iota)\,. \tag{6.3}$$

In this coordinate system the shadowed area is symmetric with respect to reflection at the (X, Z) and (Y, Z) planes.

In order to take into account shadowing in the radiation law (3.5) (we shall not consider re-radiation at the moment) we have to extend the region of integration only over the fraction of the crater area which is not shadowed. Thus we obtain integrals of the form

$$\int_{\text{unshad.}} \mathrm{d}f \ldots = \int_{\text{crater}} \mathrm{d}f \ldots - \int_{\text{act. shd.}} \mathrm{d}f \ldots - \int_{\text{app. shd.}} \mathrm{d}f \ldots . \tag{6.4}$$

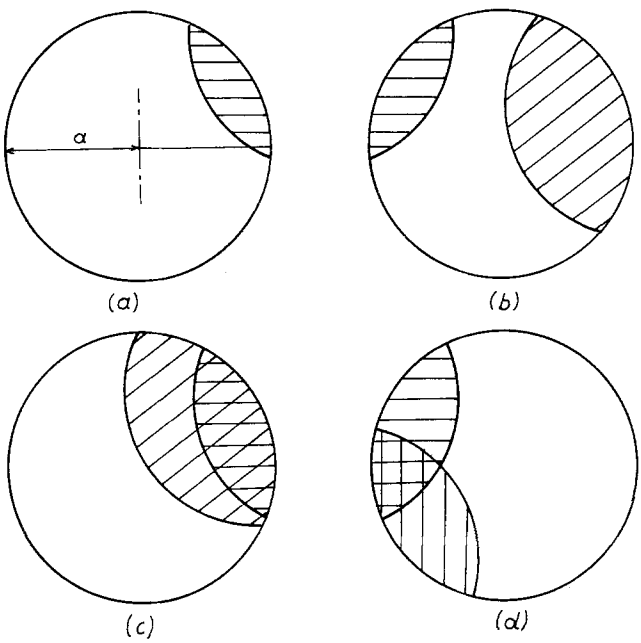

Fig. 7. Relative position of shadows.

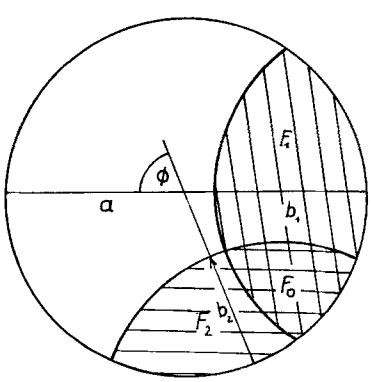

Fig. 8. Definition of overlap regions.

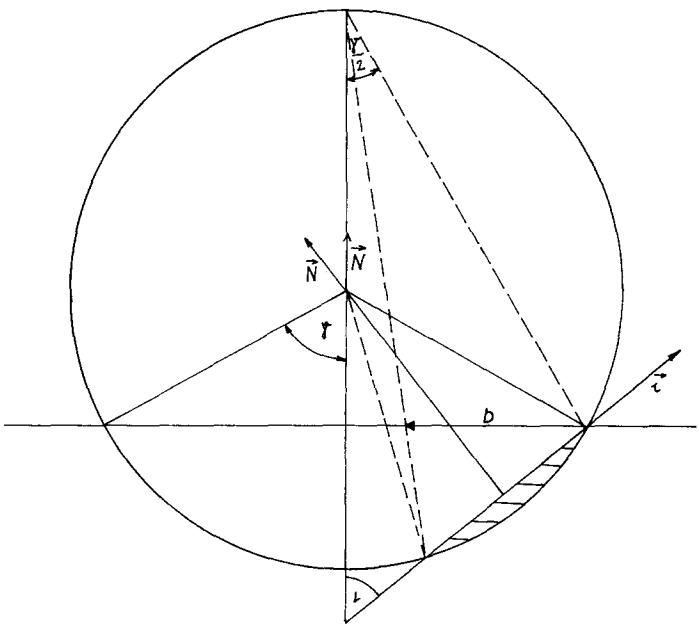

Fig. 9. Projection of the shadowed area into the XY-plane.

The integration over the total crater area has already been performed. Introducing the tensor calculus used before, we now have to evaluate integrals of the form

$$\int_{\text{shd.}} \mathrm{d}f\, n_k n_m \quad \text{and} \quad \int_{\text{shd.}} \mathrm{d}f\, n_k n_m n_r . \tag{6.5}$$

Since the shadowed area is not rotation invariant around the $\mathbf{N}'$-axis we have to make a more general ansatz for the tensors (6.5) than the one used in Section 3. We put

$$\int_{\text{shd.}} \mathrm{d}f\, n_k n_m = A_1 \hat{Z}_k \hat{Z}_m + A_2 \hat{X}_k \hat{X}_m + A_3 \hat{Y}_k \hat{Y}_m , \tag{6.6}$$

and

$$\int_{\text{shd.}} \mathrm{d}f\; n_k n_m n_r = B_1 \hat{Z}_k \hat{Z}_m \hat{Z}_r + B_2 (\hat{Z}_k \hat{X}_m \hat{X}_r + \hat{Z}_m \hat{X}_k \hat{X}_r + \hat{Z}_r \hat{X}_k \hat{X}_m) + B_3 (\hat{Z}_k \hat{Y}_m \hat{Y}_r + \hat{Z}_m \hat{Y}_k \hat{Y}_r + \hat{Z}_r \hat{Y}_k \hat{Y}_m) . \tag{6.7}$$

All linear terms in $\hat{X}$, $\hat{Y}$ vanish because of reflection symmetry. The coefficients A_k, B_k $k = 1, 2, 3$ can be obtained as before by contracting with the appropriate tensors. Not all of these constants will be needed, however, since the tensor (6.6) enters in (3.6) only in the combination

$$i_k e_m \int_{\text{shd.}} \mathrm{d}f\; n_k n_m = A_2 (\mathbf{i} \cdot \hat{\mathbf{X}}) (\mathbf{e} \cdot \hat{\mathbf{X}}) = A_2 \cos\alpha , \tag{6.8}$$

so that only A_2 enters in the calculation of the radiation. A_2 can be calculated from

$$A_2 = \int_{\text{shd.}} \mathrm{d}f \; n_X{}^2 = sFv_i, \tag{6.9}$$

where the shadowing function v_i is defined by

$$v_i = \frac{1}{sF} \int_{\text{shd.}} \mathrm{d}f \; n_X{}^2 = v(\cos \iota, s). \tag{6.10}$$

For apparent shadowing we have to use the function

$$v_e = v(\cos \varepsilon, s), \tag{6.11}$$

i.e., the same function but of a different argument. The function $v(\cos \iota, s)$ will be calculated together with the other shadowing function w in the appendix. They can be computed by straightforward, but rather lengthy integrations.

For the non-Lambertian part of the radiation we proceed analogously. The tensor (6.7) appears in (3.6) only in the combination

$$i_k e_m e_r \int_{\text{act. shd.}} \mathrm{d}f \; n_k n_m n_r = 2B_2 (\mathbf{e} \cdot \hat{\mathbf{Z}}) (\mathbf{e} \cdot \hat{\mathbf{X}}) \tag{6.12}$$

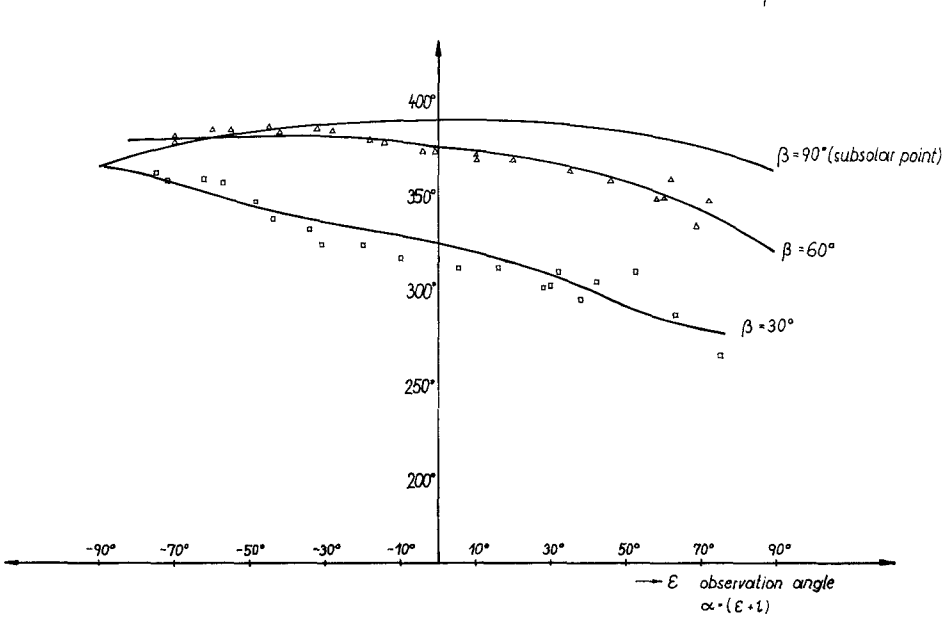

Fig. 10. Comparison with experiment – Coplanar data at 90°, 60° and 30° solar elevation.

for actual shadowing, and in the combination

$$i_k e_m e_r \int_{\text{app. shd.}} \mathrm{d}f\ n_k n_m n_r = B_2\,(\mathbf{i}\cdot\hat{\mathbf{Z}}') \tag{6.13}$$

for apparent shadowing where the coordinate system (6.3) is now defined with **e** rather than **i** as relevant direction. This has been indicated by the notation $\hat{\mathbf{Z}}'$. It is this freedom in the choice of the coordinate system which is one of the major advantages of the tensor formalism used here.

The scalar products $(\mathbf{e}\cdot\hat{\mathbf{Z}})$ and $(\mathbf{i}\cdot\hat{\mathbf{Z}})$ resp. can be computed from (6.3) to be

$$\begin{aligned}(\mathbf{e}\cdot\hat{\mathbf{Z}}) &= (\cos\varepsilon - \cos\alpha\cos\iota)/\sin\iota\,,\\ (\mathbf{i}\cdot\hat{\mathbf{Z}}') &= (\cos\iota - \cos\alpha\cos\varepsilon)/\sin\varepsilon\,,\end{aligned} \tag{6.14}$$

while $(\mathbf{e}\cdot\hat{\mathbf{X}}) = \sin\alpha$.

The coefficient B_2 will be calculated in the appendix in terms of the shadowing function w, defined by

$$B_2 = \int_{\text{act. shd.}} \mathrm{d}f\ n_X{}^2 n_z = sF\sin\iota\, w_i\,, \tag{6.15}$$

where $w_i = w(\cos\iota, s)$. For apparent shadowing the calculation proceeds analogously, the function w_i being replaced by $w_e = w(\cos\varepsilon, s)$.

This completes the calculation of the energy radiated from a partially shadowed crater in the approximation that re-radiation corrections have been neglected. The radiation becomes

$$\begin{aligned}E(\mathbf{e},\mathbf{i},\mathbf{N}) = \frac{S_c}{\pi}\{&\cos\alpha\,(1-r)\,s[(1-2s/3)/(1-s) - v_i - v_e]\\ &+ (1-r)\cos\varepsilon\cos\iota\,(1-2s) + 3rs\,(1-s-w_e)\cos\iota/2\\ &+ 3rs\,(1-s-w_i+\tfrac{1}{2}w_e)\cos\alpha\cos\varepsilon + 3rsw_i\cos^2\alpha\cos\iota\\ &+ 3r\,(1-5s+5s)\cos\iota\cos^2\varepsilon/2\}.\end{aligned} \tag{6.16}$$

The re-radiation contributions have to be added to this expression for the energy flux. Before we can do this we have to correct these contributions for the influence of shadowing. When part of the crater is shadowed the m-th order re-radiation contribution becomes

$$\begin{aligned}\mathrm{d}^{(m)}E = S_c\frac{1}{F}\int \mathrm{d}f_0\,(\mathbf{i}\cdot\mathbf{n}_0)\,(1-r+3rr_{01}/4R)\\ \times\left[\int\frac{\mathrm{d}f_0}{4\pi R^2}\,(1-r+3rr_{12}/4R)\right]^{m-1}\varrho\,(\mathbf{e},\mathbf{n}_m)\,\mathrm{d}f_m/4\pi R^2\,.\end{aligned} \tag{6.17}$$

The intermediate integrals have to be extended over the whole crater as before. These integrals can be carried out, using the same approximations as in the evaluation of (5.1), i.e. we neglect terms of order $rs^{5/2}$, which amounts to replacing $r_{k,k+1}$ in the

intermediate integrals by its average value. The m-th order contribution becomes, therefore,

$$\mathrm{d}^{(m)} E = S_c (1 - s) K^m \int \mathrm{d}f_0 (\mathbf{i} \cdot \mathbf{n}_0) \frac{1}{F} \int \mathrm{d}f_m \varrho (\mathbf{e}, \mathbf{n}_m), \tag{6.18}$$

where K is defined by (5.4). The first and last integrals in (6.18) are influenced by shadowing, however, and have to be considered in detail. The first integral $\int \mathrm{d}f_0$ has to be extended over the area which is not actually shadowed (apparent shadowing does not influence this integral, since the invisible area contributes to re-radiation).

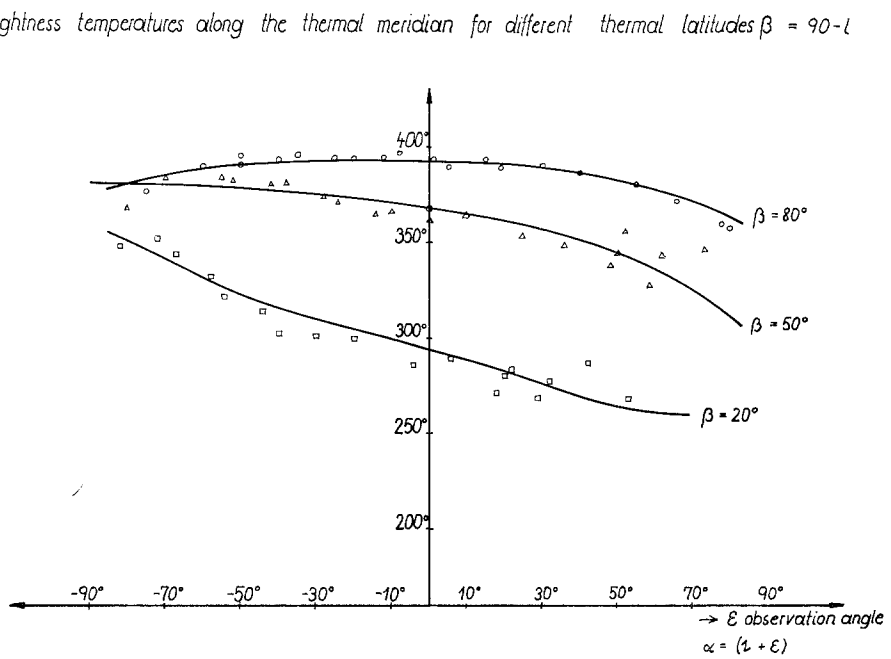

Fig. 11. Comparison with experiment – Coplanar data at 80°, 50° and 20° solar elevation.

The contribution of actual shadowing would, however, be proportional to

$$\int \mathrm{d}f \; n_k = \text{const} \; \hat{\mathbf{Z}}_k \; ; \tag{6.19}$$

and the scalar product $i_k \hat{\mathbf{Z}}_k$ needed in (6.18) vanishes. The first integral can thus be extended over the whole crater and we obtain

$$\int \mathrm{d}f_0 (\mathbf{i} \cdot \mathbf{n}_0) = F \cos \iota \, . \tag{6.20}$$

The only re-radiation integral influenced by shadowing is therefore the last one, i.e. the integration $\int \mathrm{d}f_m$. Here we have to take into account that part of the crater will

be invisible from the direction of observation and the re-radiation emitted by this part has to be subtracted from the re-radiation. The relevant integrals become

$$e_k \int_{\text{app. shd.}} \mathrm{d}f \; n_k = \text{const}\; e_k \hat{\mathbf{Z}}_k' = 0 \tag{6.21}$$

and

$$e_k e_m \int_{\text{app. shd.}} \mathrm{d}f \; n_k n_m = A_2 = sFv_e \,. \tag{6.22}$$

This is the only modification of the re-radiation contribution due to shadowing. Inserting (6.22) into (6.18) and summing the infinite series we obtain

$$E^r = \frac{S_c K(1-s)}{\pi(1-K)} \cos\iota \left\{ (1-r)\cos\varepsilon + \frac{3r}{2}\left[s\left(\frac{1-2s/3}{1-s} - v_e \right) + (1-2s)\cos^2\varepsilon \right) \right\}. \tag{6.23}$$

This expression replaces (5.6) and has to be added to (6.16).

The resulting expression for the energy flux is valid in cases (a) and (b) of the classification of the shadowing situations given above. In case (c) only the shadowing functions belonging to the larger shadow have to be considered, while the other shadowing functions have to be put equal to zero.

Brightness temperature along the thermal meridian for different thermal latitudes $\beta = 90 - l$

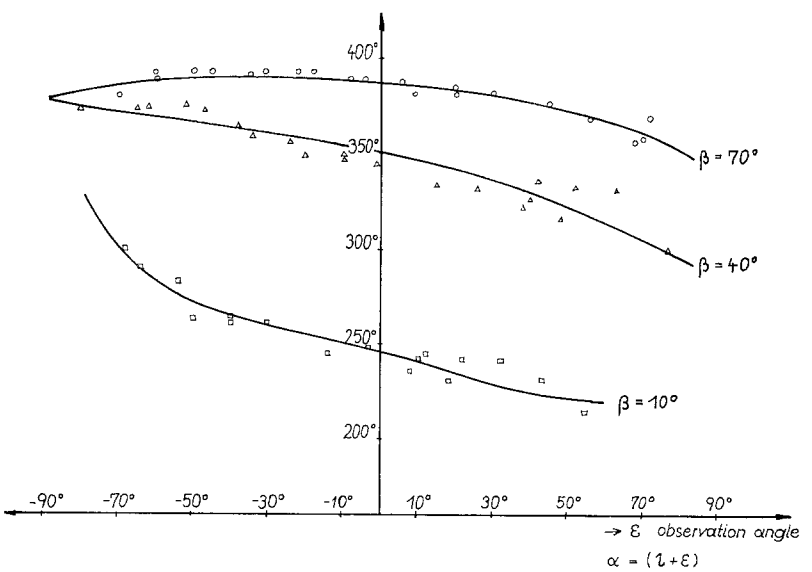

Fig. 12. Comparison with experiment – Coplanar data at 70°, 40° and 10° solar elevation.

In case (d), when both shadows overlap only partially an extremely complicated geometrical situation arises which can be dealt with only approximately. The approximation procedure has to fulfil several requirements, listed below, and the following approach has turned out to be the best (see Figures 8 and 9).

The shadowed areas are projected stereographically on the plane through the crater rim and the resulting areas are denoted by F_1, F_2 and F_0 resp. for the projections of the apparent shadow, actual shadow and overlap resp. Then we replace the shadowing functions by the following new functions

$$v_i + v_e \to (v_i + v_e)\left(1 - \frac{F_0}{F_1 + F_2}\right), \tag{6.24}$$

$$w_i \to w_i(1 - F_0/F_1). \tag{6.25}$$

This ensures that the sum of two shadowing functions does not exceed the limiting value corresponding the total shadowing of the crater. The temperatures at large angles of observation are, furthermore, very sensitive to the exact manner in which w_e and v_e approach their limiting values as $\varepsilon \to \pi/2$. By using the approximation (6.25) and leaving v_e and w_e unchanged one ensures that this limiting value is unaffected by the approximations used here.

We have checked the approximations (6.24, 25), furthermore, in the case where **i**, **e** and **N** are coplanar (i.e. along the lunar equator). In this case the overlap situation

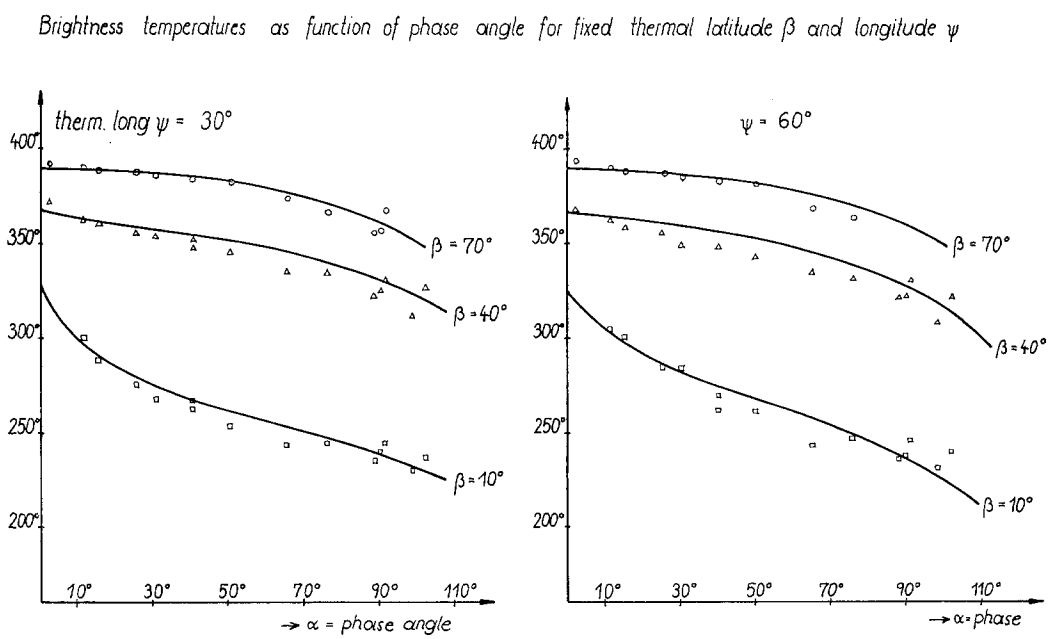

Fig. 13. Off-equator data I.

can be dealt with exactly with the help of the tensor techniques developed in Section 3. The differences between exact result and approximate equation are smaller than 3 K at all angles of observation.

The only remaining task is the calculation of the areas F_1, F_2 and F_0. These areas can be computed with the help of standard geometrical formulas. The resulting equations are, however, extremely complicated and will not be given here explicitly.

7. Comparison with Experiment

We are now in a position to compare our theoretical results with the experimental measurements. Adding (6.23) to (4.6) we obtain for the energy radiated by a unit surface element per unit time and solid angle

$$\begin{aligned} E(\varepsilon, \iota, \alpha) &= E(\mathbf{e}, \mathbf{i}, \mathbf{N}) + E^r(\mathbf{e}, \mathbf{i}, \mathbf{N}) \\ &= \frac{S_c}{\pi}(1-r)\left\{\left[1 - 2s + \frac{K(1-s)}{1-K}\right]\cos\varepsilon\cos\iota\right. \\ &\quad + s\left[\frac{1-2s/3}{1-s} - (v_i + v_e)\left(1 - \frac{F_0}{F_1+F_2}\right)\right]\cos\alpha\Big\} \\ &\quad + \frac{S_c}{\pi}\frac{3r}{2}\left\{\left[1 - 5s + 5s + (1-2s)\,K\,\frac{1-s}{1-K}\right]\cos\iota\cos^2\varepsilon\right. \\ &\quad + s\left[1 - s - w_e + \frac{K}{1-K}(1 - 2s/3 + sv_e - v_e)\right]\cos\iota \\ &\quad + 2s\left[1 - s - w_i(1 - F_0/F_1) + \tfrac{1}{2}w_e\right]\cos\alpha\cos\varepsilon \\ &\quad \left. + 2sw_i(1 - F_0/F_1)\cos^2\alpha\cos\iota\right\}. \end{aligned} \tag{7.1}$$

The apparent temperature of the lunar surface is related to $E(\varepsilon, \iota, \alpha)$ by

$$T^4 = \frac{\pi}{\cos\varepsilon} E(\varepsilon, \iota, \alpha). \tag{7.2}$$

In order to get some ideas on the parameters r and s to be inserted into (7.1) we calculate first the temperature of the subsolar point at zero phase-angle, which is known experimentally to be 397 K. We obtain

$$T^4(0, 0, 0) = \frac{S_c}{\pi}\left[1 + \frac{1}{2}r - \frac{5}{2}rs + \frac{s^2}{3(1-s)} + 0(rs^2)\right]. \tag{7.3}$$

The factor S_c/π corresponds to a temperature of 390 K (or to 385 K if we assume an albedo of 0.08), the factor in square brackets in (7.3) has thus to be approximately 1.10. This can be obtained either by putting $r=0.20$, $s=0$ or $r=0$ and $s=0.4$ or by a suitable combination of both non-Lambertian terms and roughness effects.

Our theoretical Expression (7.1, 2) has been evaluated for a large number of crater

Brightness temperature as function of phase angle for fixed thermal latitude β and longitude ψ

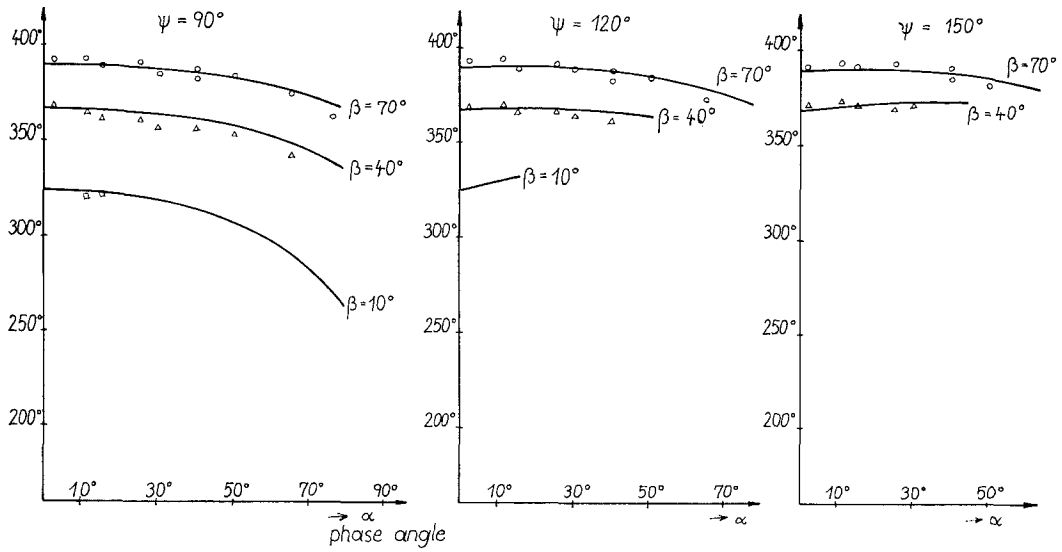

Fig. 14. Off-equator data II.

distributions and values of r by means of a computer and a statistical analysis of the data has been performed. The total χ^2 has been calculated for each fit, ascribing to the experimental data of Saari and Shorthill a formal error of ± 10K. The rms deviation between theory and experiment has also been computed for each case. We have fitted both a representative sample (151 data) of the measurements along the lunar equator as well as a total of 526 data distributed evenly over all values of ι, ε and α. The results are shown in Table II.

The table shows that the best fit to the data is achieved for model C as far as the coplanar data are concerned and for model E when all data are considered. Model E has the disadvantage, however, that the temperature of the subsolar point comes out to be only 392K at full Moon which is unacceptably low. Therefore, model A has been chosen as the best fit for all lunar data. The table shows, however, that the quality of different fit is not too different and that excellent results can be achieved with a wide variety of lunar surface models.

Especially simple theoretical expressions for the lunar surface temperatures are obtained when models E, B or F are used. For numerical calculations is therefore best to use the simple fit E, which agrees with the lunar surface model suggested first by Buhl *et al.* (1968). The non-Lambertean parameter r does not lead to a very substantial improvement of the explanation of the emperical data and one can conclude therefore that the assumption that a flat element of the lunar surface is a Lambertean radiator is in good agreement with experiment.

TABLE II

Comparison of theory with the Saari Shorthill data

Model	Coplanar data		All data		$T(0, 0, 0)$
	x^2	rms	x^2	rms	
A	54.8	0.170	184.0	0.168	394.6
B	40.1	0.152	215.8	0.172	396.7
C	37.5	0.148			396.8
D	54.5	0.175	165.4	0.164	390.5
E	38.2	0.154			392.6
F	47.0	0.160			391.8

Description of models:

A...albedo 5% $r=0.15$ $s=(0.3$ 50% 0.013 50%)
B...albedo 5% $r=0.0$ $s=(0.49$ 45% 0.01 55%)
C...albedo 5% $r=0.05$ $s=(0.49$ 45% 0.01 55%)
D...albedo 10% $r=0.15$ $s=(0.3$ 50% 0.013 50%)
E...albedo 10% $r=0.0$ $s=(0.49$ 45% 0.01 55%)
F...albedo 10% $r=0.0$ $s=(0.49$ 33% 0.2 33%
0.01 34%)

$$x^2 = \sum_{i=1}^{N} \left(\frac{T_{i\,\mathrm{exp}} - T_{i\,\mathrm{theor.}}}{10} \right)^2 \qquad \mathrm{rms} = \left(\frac{1}{N} \sum_{i=1}^{N} \frac{|T^2_{i\,\mathrm{exp}} - T^2_{i\,\mathrm{theor.}}|}{T^2_{i\,\mathrm{exp}}} \right)^{1/2}$$

$N=151$ coplanar data, 526 all data.

Acknowledgements

Our thanks are due to J. Harrison and B. Jones for many valuable suggestions and to Dr H. Urbantke for his analysis of the crater geometry. Dr J. Nance has participated in the initial stages of this work.

References

Ashby, N.: 1967, *Publ. Astron. Soc. Pacific* **78**, 254.
Buhl, D., Welch, W. J., and Rea, J.: 1968, *J. Geophys. Res.* **73**, 5281.
Hammermesh, M.: 1962, *Group Theory*, Addison Wesley, Cambridge, Mass.
Pettit, E. and Nicholson, S. B.: 1930, *Astrophys. J.* **71**, 102.
Saari, J. M. and Shorthill, R. W.: 1967, 'Isothermal and Isophotic Atlas of the Moon', NASA Rep. CR-855 (Sept.).
Smith, B. G.: 1967, *J. Geophys. Res.* **72**, 4059.
Winter, D. F. and Krupp, J. A.: 1970, Boeing Sci. Res. Laboratories, Report No. D1-82-0987 (July).

Appendix: Calculations of the Shadowing Function

The shadowing functions v and w defined before are of the general type ($h_0=v$, $h_1=w$)

$$h_m(\cos\iota, s) = \frac{1}{Fs \sin^m \iota} \int_{\text{shd.}} \mathrm{d}f \; n_X{}^2 n_Z{}^m . \tag{A.1}$$

The integrals have to be extended over the shadowed area of the crater, i.e. over a wedge of a sphere. Note that the directions X and Z refer to the coordinate system defined in (6.3) and that the region of integration is thus symmetric with respect to the (X, Z) and (Y, Z) planes. For simplicity, we have dropped the bar over the axes.

The region of integration is bordered by the crater edge and the edge of the shadow resp. as shown in Figure 6. The equation of the crater rim is given by the intersection of a plane with a sphere

$$z = R\cos\gamma, \qquad x^2 + y^2 + z^2 = R^2 . \tag{A.2}$$

In the (X, Y, Z) system the sphere remains unchanged while the equation of the plane is given by

$$-X\cos\iota + Z\sin\iota = R\cos\gamma . \tag{A.3}$$

The other border of the shadow is then obtained by the substitution $X \to -X$. Because of the symmetry of the shadowed area shown in Figure 6, it will suffice to integrate over one quarter of the shadowed area only, i.e. only in the region $X>0$, $Y>0$.

Introducing polar coordinates by

$$Z = R\cos\theta, \qquad X = R\sin\theta\cos\phi, \qquad Y = R\sin\theta\sin\phi , \tag{A.4}$$

the equation for the crater rim becomes

$$\cos\theta_R \sin\iota - \sin\theta_R \cos\iota \cos\phi = \cos\gamma . \tag{A.5}$$

This equation can be solved for $\xi_R = \cos\theta_R$ as

$$\xi_R = [\cos\gamma \sin\iota + \cos\phi \cos\iota \sqrt{\sin^2\gamma - k^2}]/(1 - k^2), \tag{A.6}$$

where

$$k = \cos\iota \sin\phi . \tag{A.7}$$

In terms of these variables the surface element $\mathrm{d}f$ becomes $\mathrm{d}f = R^2 \,\mathrm{d}\phi\mathrm{d}\xi$. To evaluate (A.1) we need, furthermore, the directional cosines

$$n_X = \cos\phi \sin\theta = \cos\phi \sqrt{1 - \xi^2}, \qquad n_Z = \cos\theta = \xi . \tag{A.8}$$

The integrals (A.1) thus become

$$h_m(\cos\iota, s) = \frac{4R^2}{\sin^m \iota 4\pi R^2 s^2 (1 - s)} \int_0^{\pi/2} \mathrm{d}\phi \cos^2\phi \int_{\xi_R}^{1} \mathrm{d}\xi \, \xi^m (1 - \xi^2) .$$

$$m = 0, 1 \tag{A.9}$$

The factor 4 in the numerator is due to the fact that we integrate in (A.9) only over one quarter of the shadowed area, as discussed before. The integral over ξ can be

carried out without difficulty, leading to integrals of the general type

$$I_m = \int_0^{\pi/2} \mathrm{d}\phi\,(1 - \xi_R^m) = \int_0^{\pi/2} \mathrm{d}\phi\,\{1 - [(\cos\gamma \sin\iota + \cos\phi \cos\iota \sqrt{\sin^2\gamma - k^2})/(1 - k^2)]\}^m . \tag{A.10}$$

These integrals can be evaluated analytically. Putting

$$p = \cos\iota, \qquad q = \sqrt{\sin^2\gamma - \cos^2\iota} = \sqrt{4s(1-s) - p^2}, \tag{A.11}$$

and introducing the abbreviations

$$A = \frac{1}{\pi}\operatorname{arctg}\frac{q}{p}, \qquad B = \frac{1}{\pi}\operatorname{arctg}\frac{q}{p(1-2s)}, \tag{A.12}$$

we obtain

$$\begin{aligned} v(p, s) = h_0 &= 2B\left[\frac{1 - 2s/3}{1-s} + \frac{p^2}{s}(1-2s)\right] \\ &\quad + \frac{1}{3s^2(1-s)}\left\{A - B + \frac{pq}{2\pi}(1 - 12s + 12s^2)\right\}, \\ w(p, s) = h_1 &= 2B\left[1 - s + \frac{p^2}{s}(1 - 5s + 5s^2)\right] \\ &\quad + \frac{pq(1-2s)}{4\pi s}\left[\frac{q^2}{3s(1-s)(1-p^2)} - 10\right]. \end{aligned} \tag{A.13}$$

This completes the evaluation of the shadowing functions.